LASER INTERFEROMETER GRAVITATIONAL WAVE OBSERVATORY
- LIGO -
CALIFORNIA INSTITUTE OF TECHNOLOGY
MASSACHUSETTS INSTITUTE OF TECHNOLOGY

Technical Note	LIGO-T1800224–v0	2018/07/27

Physical and statistical analysis of scatter in Fabry-Pérot arm cavity of Advanced LIGO
- Interim Report 2 -

SURF Students: Wenxuan Jia, Mentor: Anamaria Effler, Valery Frolov

California Institute of Technology
LIGO Project, MS 18-34
Pasadena, CA 91125
Phone (626) 395-2129
Fax (626) 304-9834
E-mail: info@ligo.caltech.edu

Massachusetts Institute of Technology
LIGO Project, Room NW22-295
Cambridge, MA 02139
Phone (617) 253-4824
Fax (617) 253-7014
E-mail: info@ligo.mit.edu

LIGO Hanford Observatory
Route 10, Mile Marker 2
Richland, WA 99352
Phone (509) 372-8106
Fax (509) 372-8137
E-mail: info@ligo.caltech.edu

LIGO Livingston Observatory
19100 LIGO Lane
Livingston, LA 70754
Phone (225) 686-3100
Fax (225) 686-7189
E-mail: info@ligo.caltech.edu

http://www.ligo.caltech.edu/

Abstract

In the dual-recycled Michelson interferometer of Advanced LIGO, the optical scatter exists in the resonant Fabry-Pérot arm cavities due to imperfections of test mass surface. We studied scatter in observation run 2 with measurements of photo diodes on the arm cavity baffle, and investigated its relation with other factors sampled from auxiliary data channels. The steady-state scatter during locks of interferometer is analyzed and compared with FFT-based simulation. Regression analysis with informed knowledge from simulation is carried out to the transient scatter measurements, during which the main beam moves on the test masses by the alignment system. With the regression model, the beam position on test mass can be inferred from scatter distribution on baffle and cross-calibrated with dither-based methods. The scatter with the new end test mass installed can be predicted for the upcoming observation run 3.

1   Introduction

In Advanced LIGO, the scattered light in the resonant Fabry-Pérot (FP) cavity, for example the low-angle scatter caused by unevenness of the high-reflection (HR) surface of the test mass, generates noise in the differential arm (DARM) signal that contains the gravitational wave (GW) information [1]. In this project, we aim at understanding the data measurements of scatter and exploring applications with such information. Regression analyses are done on couplings between scatter with other physical quantities in Observation Run 2, for example main beam position and time, to provide fundamentals for future applications.

2   Materials & Methods

2.1   Fabry-Pérot cavity scatter measurement

To prevent scattered photons from re-entering the main beam of interferometer, multiple light baffles are mounted on beam paths as shown in Figure 1.
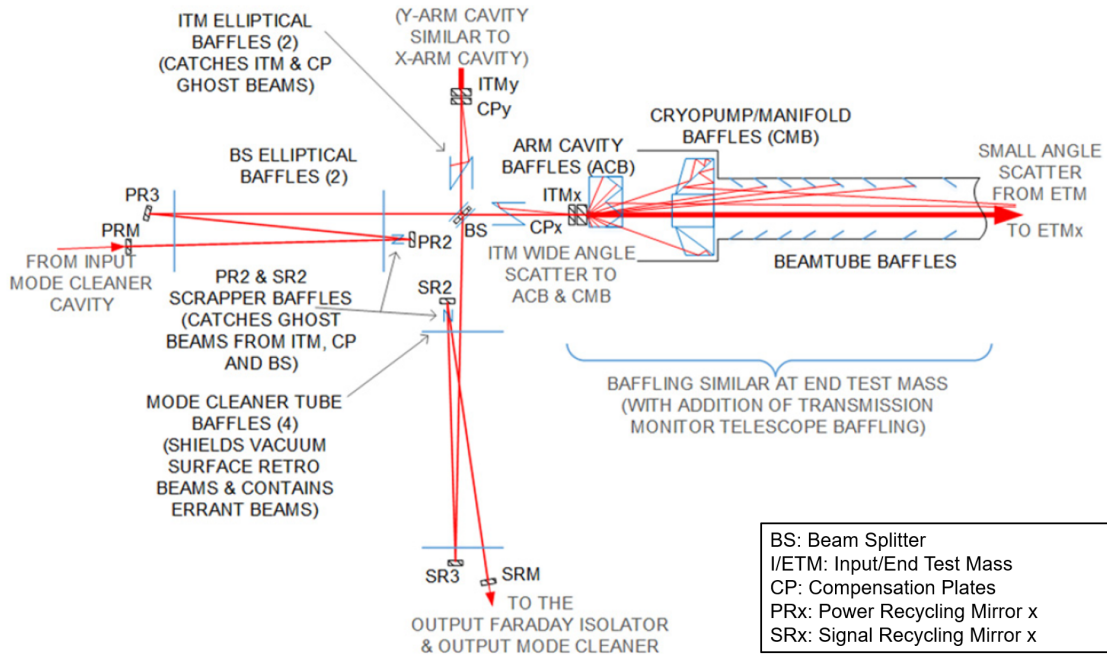

Figure 1: Locations of scattered light baffles in the LIGO optical configuration [2].

Those beamtube baffles mounted on the sidewalls of the ultra-high vacuum cavity as well as the cryopump/manifold baffles are meant to block the large-angle scatter. The low-angle scatter from the far test mass (4 km away) is caught by the arm cavity baffle (abbreviated as baffle) placed in front of each test mass optic [2]. There are four *Excelitas YAG-444-AH* photo diodes (PD) mounted on each baffle of the test mass to measure the intensity of low-angle scattered light from the test mass on the other side of FP cavity. The configurations of PD are pictured in Figure 2.
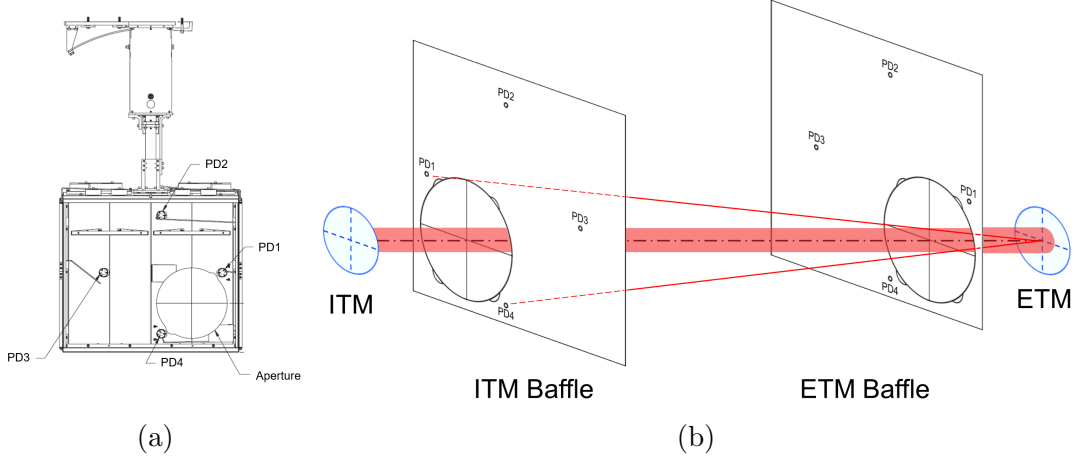
(a)
(b)

Figure 2: Schematics of the baffle PD measuring low-angle scatter. (a) the front view of the baffle with four PD mounted (Note that PD 1 and 4 are closer to aperture than Pd 2 and 3. Credit: Jose Chavez [3]). (b) FP cavity with sample ETM scatter caught on ITM baffle PD 1 and 4. The shaded line is resonant main beam and the scatter paths are annotated in dashed lines. The length of the cavity is shortened and not to scale.

In the Observation run 2 (O2) from Nov. 30, 2016 to Aug. 25, 2017, all of the 16 PDs mounted on 4 baffles have measured the scatter intensity with sampling frequency of 16 Hz, and the raw data can be accessed by channels *L1:AOS-I(E)TMX(Y)_BAFFLEPD_1(2,3,4)_POWER*. The variance across photo diodes on the same baffle are calibrated to ensure valid comparison of scatter power measured by them.

2.2   Beam alignment

During O2, the test masses in the FP cavity would drift from optimal alignment failed to form resonance. The main beam was then aligned back to the correct position by the alignment dithering system (ADS) under alignment sensing control subsystem of advanced LIGO. The ADS control system detects the beam position by dithering the end test mass at low frequency $f_{dither} < 10$ Hz, which causes a peak at f_{dither} in the amplitude spectral density of DARM signal. When the beam deviates from the desired position specified by the feedforward pitch/yaw gains (*L1:SUS-I(E)TMX(Y)_L2_DRIVEALIGN_P(Y)2L_GAIN*), the demodulated amplitude at f_{dither} in DARM would change correspondingly, and the ADS error signal (the difference between the demodulated amplitude feedback and desired amplitude) would be suppressed to the steady-state zero by this control system. Thus, the transient beam alignment process provides more beam position data points and the corresponding scatter at each position. The ADS data channels are listed in Table 1.

Since the ADS error signal depends on both beam position and dithering magnitude of the end test mass, its coupling with beam position is extracted by normalizing it with respect to dithering and general feedback gain. The setting of feedforward pitch/yaw gains are not always constant for the entire O2. Thus, we start the analysis by focusing on the longest period where all feedforward gains on test masses and PR2 stay constant, which is from Feb.

Table 1: ADS channels along with descriptions. (* is 3 for I/ETMX, 4 for I/ETMY and 5 for PR2)

Descriptions	Channel Names
General feedback gain	*L1:ASC-ADS_GAIN*
Pitch dither magnitude	*L1:ASC-ADS_PIT*_OSC_CLKGAIN*
Pitch error	*L1:ASC-ADS_PIT*_DOF_INMON*
Yaw dither magnitude	*L1:ASC-ADS_YAW*_OSC_CLKGAIN*
Yaw error	*L1:ASC-ADS_YAW*_DOF_INMON*

25, 2017 to Jun. 6, 2017 in O2. During this period, there are 163 beam alignment process identified before each lock, when the laser power is 25 W and state number (*L1:GRD-ISC_LOCK_STATE_N*) is 1731. For the baffle PD data, it is normalized by the cavity power (*L1:LSC-POP_A_LF_OUTPUT*) assuming only the first-order coupling. A sample second trend of normalized data in one of the beam alignment process is shown in Figure 3.
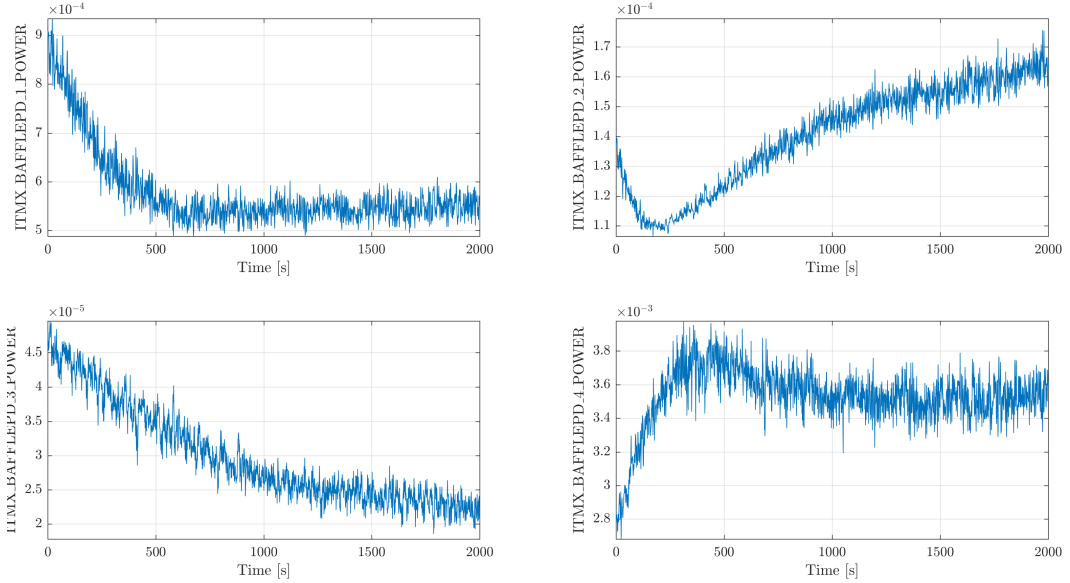
(a) ITMX PD measurements
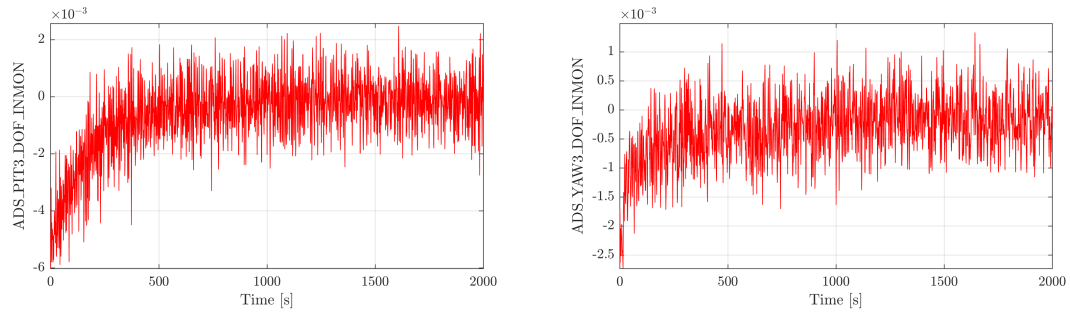
(b) ETMX pitch/yaw error signal

Figure 3: Responses of normalized ITMX PD measurements along with ADS error signal on Mar. 29, 2017

It is seen that the PD measurements change with the ADS error accordingly. Therefore, there exist correlations between scatter and beam positions at the scale of alignment. Since the PD 1 and 4 are located closer to the main beam than PD 2 and 3, their measurements are more sensitive to change of beam position as it moves from point of deviation to the same position (ADS errors gradually approach zero). Thus, much of our focus is put on the PD1 and 4 data. A 60-second lowpass moving average filter is applied to all raw data to remove high frequency noises as seen in Figure 3.

3 Results

3.1 Transient scatter during alignment

During the period in O2 (Feb. 25, 2017 - Jun. 6, 2017) in which the drive align gains of suspensions of PR2 and all test masses are constant, the deviated beam was moved back to the same target positions on the test masses during all of beam alignment processes. Thus, we can analyze the scatter with respect to beam positions that are represented in pitch/yaw errors, as shown in Figure 4.
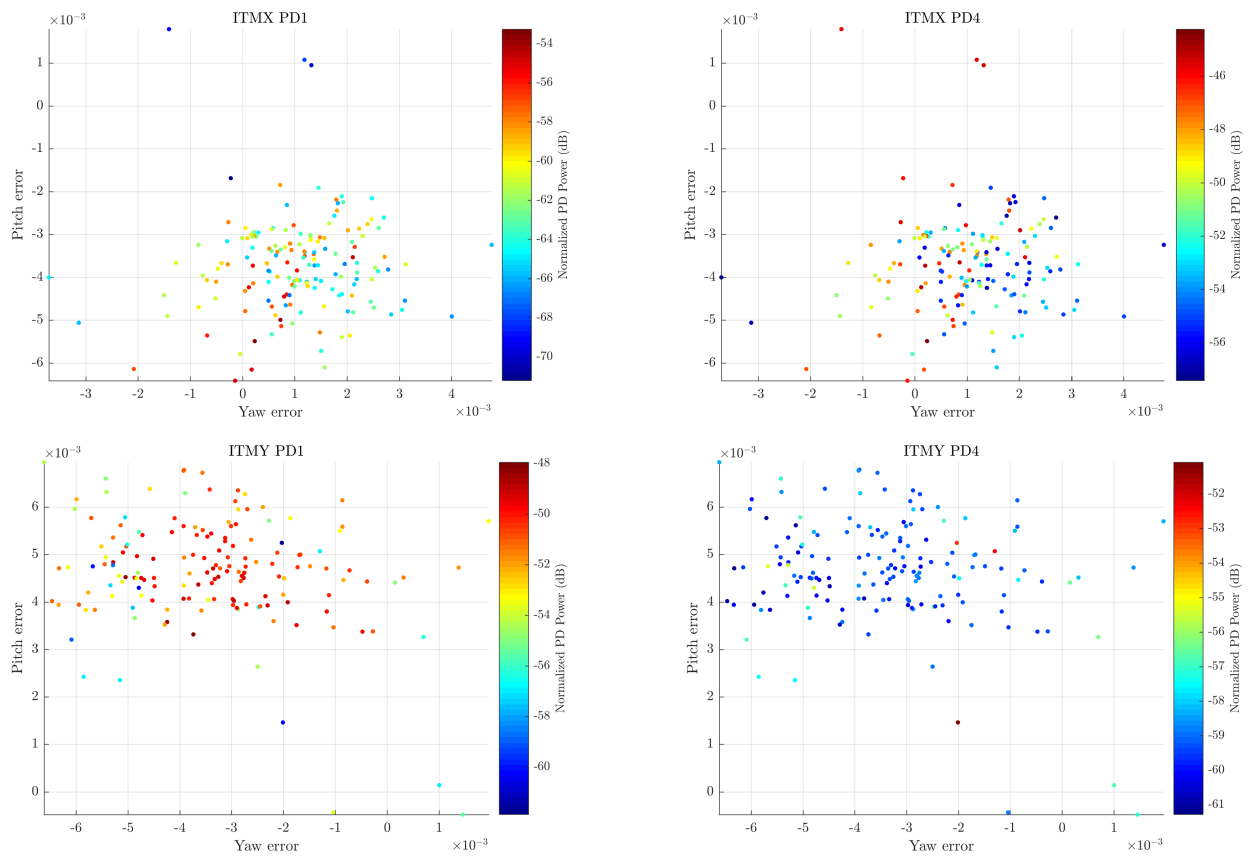

Figure 4: ITMX/Y baffle PD 1/4 measurements at the start of each beam alignment process. The color on each scatter point represents the PD power.

From the scatter plots of ITM PD, it is difficult to identify any clusters of data points that share similar power level. Nor can we identify clear coupling between PD power and beam position. The full PD trends through each alignment are presented in Figure 5 to provide an overview of scatter change in all alignments.
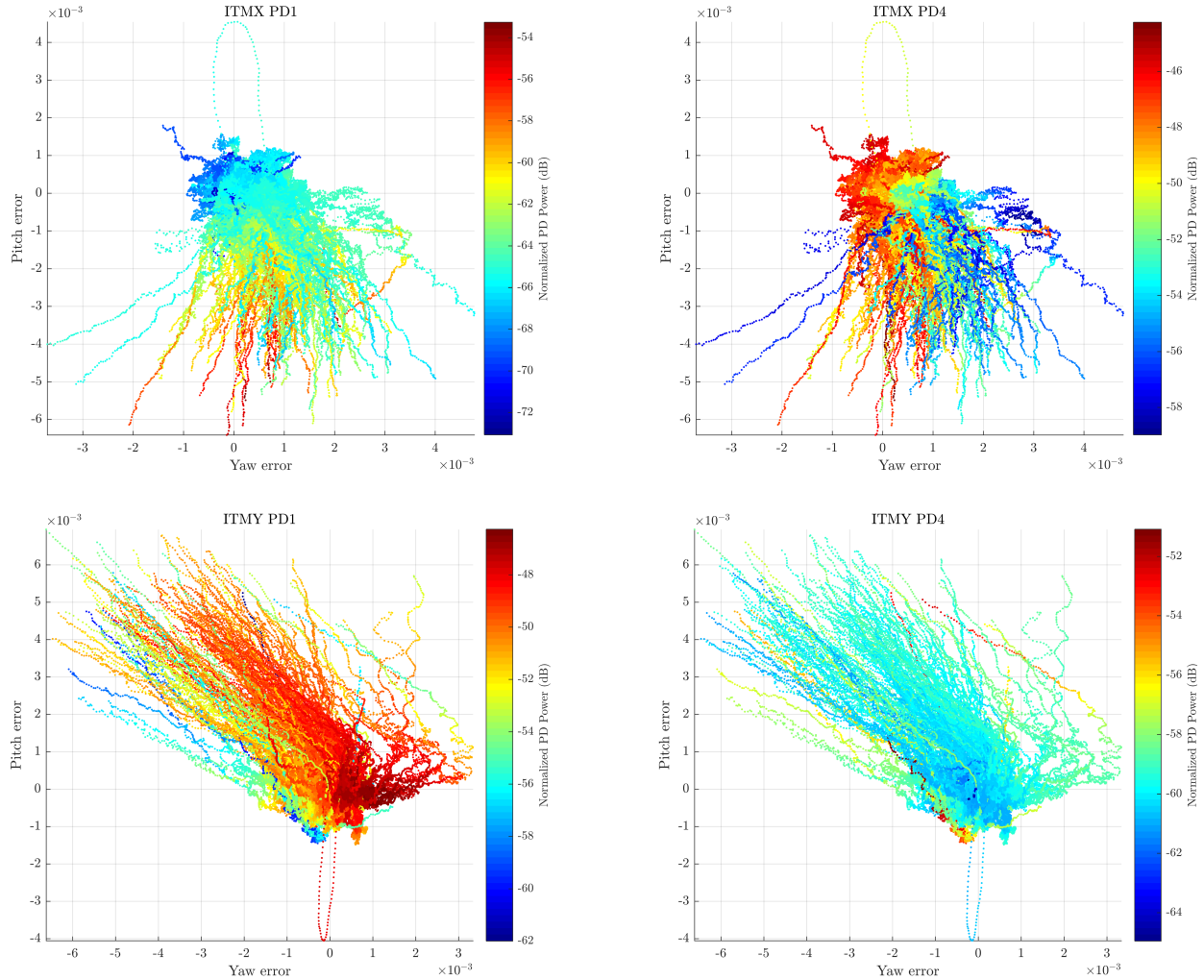

Figure 5: ITMX/Y baffle PD 1/4 measurements with respect to ADS error. Each trace of scatter represents one alignment process in which deviated beam spot was moved back to the same position (origin).

The full traces of PD measurements as beam spot returns to origin provide an overview of repeatability across all alignments. A factor of up to 5 (14 dB) difference can be seen on data points that share the same locations. It is also shown that even for very similar beam path, the corresponding scatter trend can be different by a factor up to 3 (10 dB). Specific trends are compared in Figure 6.
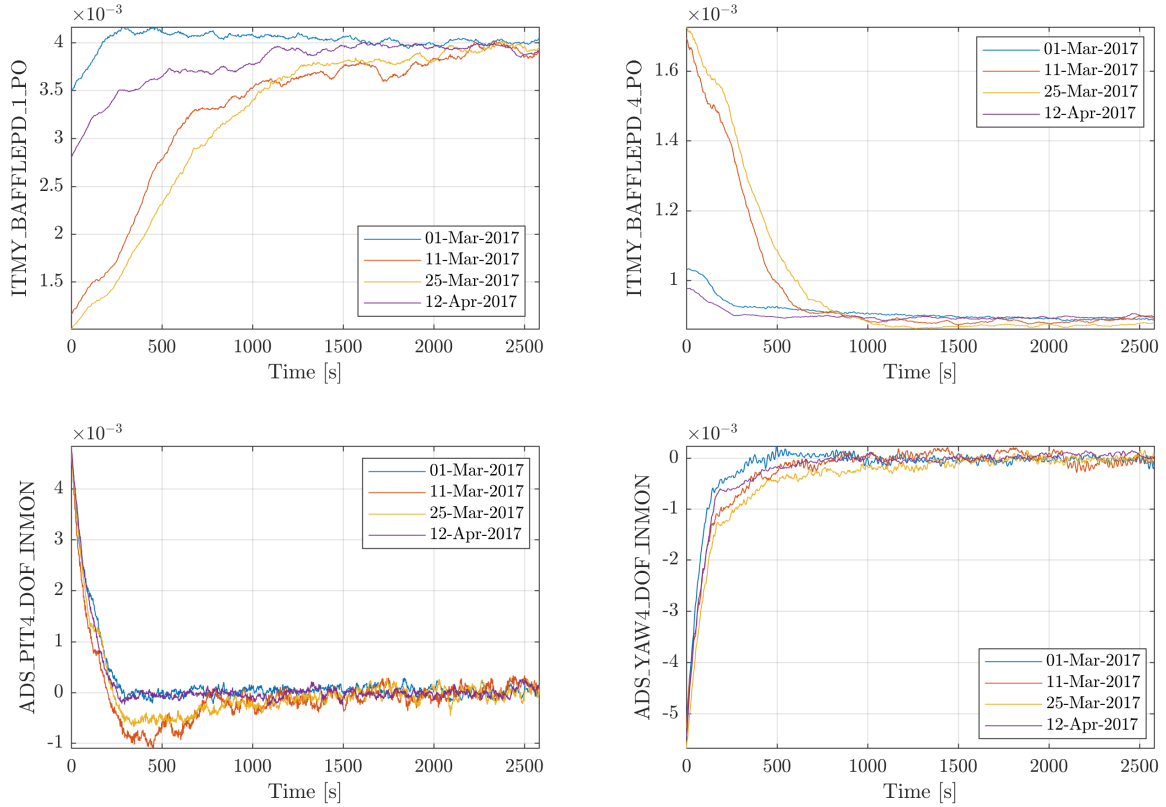
Figure 6: Trends of ITMY PD1 and 4 with respect to ETMY ADS pitch/yaw error in 4 alignment processes. The PD data are normalized by power in cavity and so are error signals. All signals are filtered with moving average of 60 seconds

Figure 6 shows 4 trends of PD response with similar beam paths from start point to the origin. Although all of PD measurement reach the same steady-state value, the variation of initial power measurements of PD1 on Mar. 1 and Mar. 25 are different by a factor of 3.5. Thus, there exist other parameters coupled with scatter other than beam position on ETM. The position of beam into the FP cavity, namely the spot position on ITM controlled by PR2, would also affect the scatter on ITM baffle. In this case, it would be difficult to directly visualize correlation as a result of higher dimensions. Thus, regression analysis is carried out to determine couplings of PD power versus beam positions on ITM and ETM.

3.2 General linear regression analysis

Extensive regression analytical methods have been developed to characterize correlations between response(s) and predictor(s). Unlike complex nonparametric modelings or neural networks, parametric regression model often can be interpreted as physical implications such as first or higher-order couplings. Among various parametric models, the general linear model is most computationally efficient given the knowledge of structure of the model. A general linear regression models the response y with p-dimensional predictors $x_i, i = 1, 2, ..., p$ as

$$y = \beta_0 + \sum_{i=1}^{K-1} \beta_i f_i(x_1, x_2, ..., x_p) + \varepsilon \tag{1}$$

where β are coefficients of each function f, and ε is the normal distributed random noise. Given n observations, the data can be represented as

$$\mathbf{y} = \mathbf{X}\boldsymbol{\beta} + \boldsymbol{\varepsilon} \tag{2}$$

where $\mathbf{X}$ is the design matrix of $\mathbb{R}^{(n \times K)}$ and the fitted coefficients $\mathbf{b}$ can be solved by ordinary least squares. For the univariate model, each row of $\mathbf{X}$ has identical structure. Consider the case of independent effects of the parameters (no interaction) with order up to k, the design matrix can be represented as

$$\mathbf{X} = \begin{bmatrix} 1 & x_{11} & x_{11}^2 & \cdots & x_{11}^k & x_{21} & \cdots & x_{21}^k & \cdots & x_{p1}^k \\ \vdots & \vdots & \vdots & & \vdots & \vdots & & \vdots & & \vdots \\ 1 & x_{1j} & x_{1j}^2 & \cdots & x_{1j}^k & x_{2j} & \cdots & x_{2j}^k & \cdots & x_{pj}^k \\ \vdots & \vdots & \vdots & & \vdots & \vdots & & \vdots & & \vdots \\ 1 & x_{1n} & x_{1n}^2 & \cdots & x_{1n}^k & x_{2n} & \cdots & x_{2n}^k & \cdots & x_{pn}^k \end{bmatrix} \tag{3}$$

where j is the jth of total n observations. In actual regression, not every order of parameter x_i reveals a strong correlation with response. In practice, a stepwise linear regression is performed to add or remove term in the design matrix based on its correlation. To characterize the coupling between baffle PD and predictors of cavity power, beam position on ITM and ETM, the stepwise linear model is trained with all alignment trends of data (size of $\sim 10^5$) for the upper bound of order of 5. The result of linearity is shown in 2.

Table 2: R-squared value of the stepwise regression result of ITM baffle PD with respect to order.

Order	ITMX				ITMY			
	PD1	PD2	PD3	PD4	PD1	PD2	PD3	PD4
1	0.437	0.377	0.105	0.517	0.531	0.665	0.390	0.292
2	0.491	0.477	0.273	0.555	0.672	0.689	0.523	0.434
3	0.500	0.505	0.282	0.594	0.699	0.705	0.531	0.457
4	0.501	0.507	0.294	0.598	0.714	0.706	0.534	0.471
5	0.511	0.512	0.314	0.602	0.714	0.707	0.534	0.484

For the model with higher-order independent parameters, the response does not follow linearly with R-squared values from 0.5 to 0.7. The addition of higher-order terms in design matrix lead to higher linearity, but the improvements are less obvious as order increases. A regression model can always be more accurate on fitting dataset as it gets arbitrarily complex, but its estimation to the future data won't necessarily improve. Thus, the interaction of parameters such as products of polynomials needs to be added to design matrix in Equation 3. The row of design matrix can be represented as:

$$\mathbf{X}_j = \begin{bmatrix} 1 & x_{1j} & \ldots & x_{1j}^{k_1} x_{2j}^{k_2} \ldots x_{pj}^{k_p} & \ldots & x_{pj}^k \end{bmatrix} \tag{4}$$

where $k_1, k_2 \ldots k_p \in \{0, 1 \ldots k\}$ and $\sum_{i=1}^{p} k_i \leqslant k$ are satisfied. Each polynomial term only appears once and k is the upper bound of order of the model. Stepwise regression is performed and the result is shown in Table 3.

Table 3: R-squared value of the stepwise regression result with respect to order. The training model has interactions.

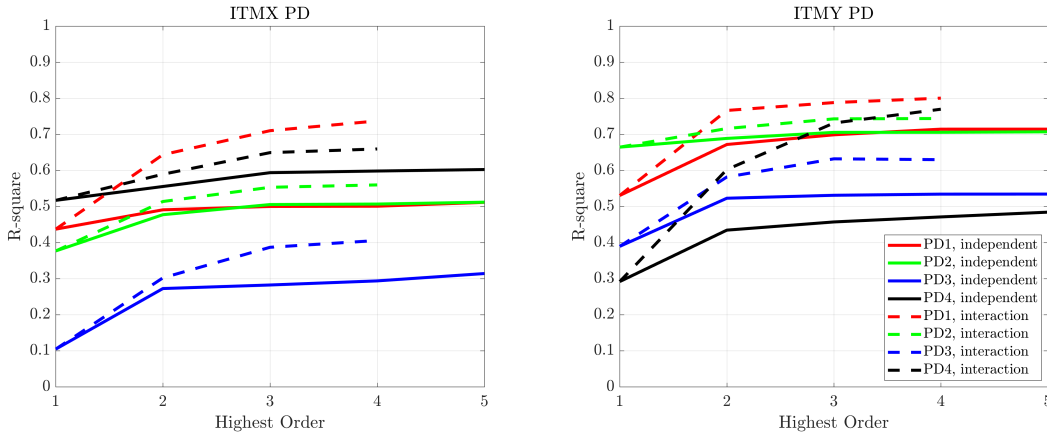| Order	ITMX				ITMY			
	PD1	PD2	PD3	PD4	PD1	PD2	PD3	PD4
1	0.437	0.377	0.105	0.517	0.531	0.665	0.390	0.292
2	0.644	0.514	0.302	0.589	0.766	0.716	0.582	0.602
3	0.710	0.553	0.387	0.649	0.788	0.743	0.632	0.731
4	0.737	0.560	0.406	0.659	0.800	0.744	0.630	0.770

Figure 7: Comparison of regression model with/out interaction terms. The R-square values are from Table 2 and 3. The legend is applied to both figures.

The new model with interactions reveals a better fitting on the data than mutually independent parameters, given the same order. The reason could be a better design matrix that is closer to the physical correlations between response and predictors, or simply the increased complexity of the model itself. However, both models exhibit latent improvement at higher-order as in Figure 7. This will be more investigated in the rest of my SURF time.

4   Next Work

The plan for the future work is listed as follows:

1. Integrate other physical modelings such as SIS [4] or other auxiliary data channels of aLIGO to the predictors of regression model.

2. Understand more complex yet effective regression models if linear or parametric models fail to make accurate predictions for the future data.

3. Extend the model to the scatter at all times of O2.

4. Improve filter algorithm to remove noises from signals, especially PR2 pitch/yaw error.

5. Calibrate PD power and position to find true BRDF.

6. Compare with new phase maps for new test masses (ETM10).

References

[1] P. Saulson, *Interferometric Gravitational Wave Detectors, 2nd Edition.* Section 6.6 pp. 99 (2017).

[2] The LIGO Scientific Collaboration, *Advanced LIGO.* Class. Quantum Grav. 32 074001 (2015).

[3] J. Chavez and E. Sanchez, *AdvLIGO SUS BSC5-L1, XYZ Local CS for SLC Arm Cavity Baffle.* LIGO-D1200677-v1.

[4] H. Yamamoto, *SIS (Stationary Interferometer Simulation) manual.* LIGO-T070039-v8.

[5] J. Rawlings, et al. *Applied Regression Analysis: A Research Tool, Second Edition.* pp. 250.